


RESEARCH ARTICLE | JUNE 10 2024

## Inductive detection of temperature-induced magnetization dynamics of molecular spin systems

Anatoly R. Melnikov  ; Mikhail Yu. Ivanov ; Arkady A. Samsonenko ; Yaroslav V. Getmanov ; Igor A. Nikovskiy ; Anna K. Matiukhina ; Ekaterina N. Zorina-Tikhonova ; Julia K. Voronina ; Alexander S. Goloveshkin; Konstantin A. Babeshkin ; Nikolay N. Efimov ; Mikhail A. Kiskin ; Igor L. Eremenko; Matvey V. Fedin ; Sergey L. Veber  



*J. Chem. Phys.* 160, 224201 (2024)  
<https://doi.org/10.1063/5.0211936>



The Journal of Chemical Physics  
2024 Emerging Investigators  
Special Collection

Submit Today

# Inductive detection of temperature-induced magnetization dynamics of molecular spin systems

Cite as: J. Chem. Phys. 160, 224201 (2024); doi: 10.1063/5.0211936

Submitted: 2 April 2024 • Accepted: 24 May 2024 •

Published Online: 10 June 2024



View Online



Export Citation



CrossMark

Anatoly R. Melnikov,<sup>1,2,a)</sup> Mikhail Yu. Ivanov,<sup>1</sup> Arkady A. Samsonenko,<sup>1,2</sup> Yaroslav V. Getmanov,<sup>2,3</sup> Igor A. Nikovskiy,<sup>4</sup> Anna K. Matiukhina,<sup>5</sup> Ekaterina N. Zorina-Tikhonova,<sup>5</sup> Julia K. Voronina,<sup>5</sup> Alexander S. Goloveshkin,<sup>4</sup> Konstantin A. Babeshkin,<sup>5</sup> Nikolay N. Efimov,<sup>5</sup> Mikhail A. Kiskin,<sup>5</sup> Igor L. Eremenko,<sup>5</sup> Matvey V. Fedin,<sup>1,2</sup> and Sergey L. Veber<sup>1,2,a)</sup>

## AFFILIATIONS

<sup>1</sup>International Tomography Center of the Siberian Branch of the Russian Academy of Sciences, 3a, Institutskaya Str., Novosibirsk 630090, Russian Federation

<sup>2</sup>Novosibirsk State University, 1, Pirogova Str., Novosibirsk 630090, Russian Federation

<sup>3</sup>Budker Institute of Nuclear Physics of the Siberian Branch of the Russian Academy of Sciences, 11, Acad. Lavrentieva Ave., Novosibirsk 630090, Russian Federation

<sup>4</sup>A.N. Nesmeyanov Institute of Organoelement Compounds of the Russian Academy of Sciences, 28, Vavilova Str., Moscow 119334, Russian Federation

<sup>5</sup>N.S. Kurnakov Institute of General and Inorganic Chemistry of the Russian Academy of Sciences, 31, Leninsky Ave., Moscow 119991, Russian Federation

<sup>a)</sup> Authors to whom correspondence should be addressed: [anatoly.melnikov@tomo.nsc.ru](mailto:anatoly.melnikov@tomo.nsc.ru) and [sergey.veber@tomo.nsc.ru](mailto:sergey.veber@tomo.nsc.ru)

## ABSTRACT

The development and technological applications of molecular spin systems require versatile experimental techniques to characterize and control their static and dynamic magnetic properties. In the latter case, bulk spectroscopic and magnetometric techniques, such as AC magnetometry and pulsed electron paramagnetic resonance, are usually employed, showing high sensitivity, wide dynamic range, and flexibility. They are based on creating a nonequilibrium state either by changing the magnetic field or by applying resonant microwave radiation. Another possible source of perturbation is a laser pulse that rapidly heats the sample. This approach has proven to be one of the most useful techniques for studying the kinetics and mechanism of chemical and biochemical reactions. Inspired by these works, we propose an inductive detection of temperature-induced magnetization dynamics as applied to the study of molecular spin systems and describe the general design and construction of a particular induction probehead, taking into account the constraints imposed by the cryostat and electromagnet. To evaluate the performance, several coordination compounds of  $\text{VO}^{2+}$ ,  $\text{Co}^{2+}$ , and  $\text{Dy}^{3+}$  were investigated using low-energy pulses of a terahertz free electron laser of the Novosibirsk free electron laser facility as a heat source. All measured magnetization dynamics were qualitatively or quantitatively described using a proposed basic theoretical model and compared with the data obtained by alternating current magnetometry. Based on the results of the research, the possible scope of applications of inductive detection and its advantages and disadvantages in comparison with standard methods are discussed.

Published under an exclusive license by AIP Publishing. <https://doi.org/10.1063/5.0211936>

## I. INTRODUCTION

There are a number of experimental techniques of paramount importance for the detailed characterization of molecular spin systems in bulk, at the single-molecule, multi- and single-layer levels. The most popular of these are alternating (AC) and direct (DC) current magnetometry,<sup>1–6</sup> electron paramagnetic resonance (EPR) spectroscopy,<sup>7–12</sup> inelastic neutron scattering,<sup>13–15</sup> and various x-ray spectroscopies.<sup>16–20</sup> In some cases, also nuclear magnetic resonance, muon spin and Mössbauer spectroscopies can provide valuable information on the physical characteristics and electronic structure.<sup>21</sup> When considering bulk dynamic properties, the gold standard for system characterization is AC magnetometry and pulsed EPR. In these techniques, the spin system under study is transferred to a nonequilibrium state either by changing the magnetic field or by applying resonant microwave pulses when the system is in a static magnetic field  $B_0$ . The perturbation creates a change in magnetic flux through the pickup coil in AC magnetometry or transverse magnetization in EPR that are detected. A sudden change in the lattice temperature of the sample also leads to a nonequilibrium population of spin levels and induces magnetization dynamics. The subsequent relaxation of the longitudinal magnetization can be tracked, for instance, by using a pickup coil, oriented parallel to  $B_0$ . From the measured kinetics, the longitudinal relaxation time can be extracted and used to evaluate the performance of a prospect spin system. For some molecular spin systems, e.g., with a total spin  $S = 1/2$ , time-resolved or pulsed EPR spectroscopy can also be used to trace the temperature-induced magnetization dynamics. Inductive detection, however, is a more general approach that can also be employed for EPR silent systems. The ubiquity of such detection is emphasized by the existence of longitudinal detection of EPR, in which the pickup coil detects the signal caused by perturbing the system with resonant microwave pulses.<sup>22–25</sup>

The original method for generating temperature jumps (T-jumps) described in Ref. 26 is based on electrical discharge of a capacitor through a conducting solution. A more robust alternative to the discharge technique is the direct heating of the sample by a powerful light pulse, which is absorbed by the solvent, matrix, or dye and converted to heat.<sup>27–30</sup> There are many different laser systems utilized as a pulsed heat source, including neodymium-doped,<sup>31,32</sup> iodine,<sup>33,34</sup> holmium,<sup>35</sup> and others that can be tuned to the desired wavelength by a stimulated Raman effect.<sup>36</sup> The majority of the laser systems operate in the visible and near-infrared frequency range and are capable of creating electronically excited transient states. In some cases, it is done purposefully, for instance, when the absorption of the pulse energy by a solvent or dye perturbs the thermal equilibrium, and the relaxation kinetics to a new equilibrium is followed. This method is popular in the investigation of various biochemical reactions and biological objects in water, in which the overtone of the OH stretching band can be excited in the near-infrared range.<sup>29</sup> In other cases where the magnetization dynamics of the compound that is excited is of interest, generated electronically excited states can interfere with the time dynamics of the perturbed but unexcited spin system. To avoid such interference, low energy quanta such as terahertz (THz), microwave, or radio frequencies should be used to irradiate the sample. This radiation interacts with the vibrational levels of the system under study or causes a temperature change due to polarization losses without generating electronically excited

states. In some cases, optical photons in the THz range could also be used to directly excite spin transitions in molecular spin systems. For instance, pulsed microwave radiation with a frequency of 118 GHz was used to study the spin dynamics in  $\text{Fe}_8$  single-molecule magnet using a Hall-probe magnetometer.<sup>37</sup> Such resonant processes can be avoided or enhanced, if necessary, by changing the frequency of the radiation used. There are many available radiation sources in the specified frequency ranges, differing in mode of operation, available power, coherence of radiation, wavelength tunability, etc.

In this paper, a THz free electron laser (FEL) of the Novosibirsk free electron laser facility is used as a source of high-power pulsed radiation with a duration of dozens of microseconds. The available spectral range of 25–111  $\text{cm}^{-1}$  (90–400  $\mu\text{m}$ ; 0.75–3.3 THz) and the average power of the THz FEL allow changing the temperature of a bulk sample without affecting its electronic state at heating rates up to 7.3  $\text{K ms}^{-1}$  even starting from liquid nitrogen temperatures.<sup>38</sup> The investigated systems are typical examples of molecular spin systems with different total spin or total angular momentum, based on the coordination compounds of  $\text{VO}^{2+}$ ,  $\text{Co}^{2+}$ , and  $\text{Dy}^{3+}$ . Various vanadium-based systems are considered as coherent systems for the realization of electronic qubits,<sup>10,11,39–42</sup> while cobalt and dysprosium coordination compounds are promising anisotropic single-molecule magnets.<sup>43–45</sup> For the mentioned three systems, we measured the magnetization dynamics and compared it with the results of AC magnetometry either qualitatively or quantitatively. This provides a comprehensive analysis of the magnetic relaxation data from both techniques and emphasizes the pros and cons of the induction method, which tracks the magnetization dynamics through a T-jump in the sample lattice. Other sections of this article include a detailed description of the detection circuit, the model of temperature-induced magnetization dynamics, a description of the radiation source and experimental setup used, and the general design and construction of the induction probehead.

## II. EXPERIMENTAL DETAILS

### A. Radiation source. Novosibirsk free electron laser facility

The Novosibirsk free electron laser (NovoFEL) facility consists of three FELs operating in the terahertz, far-infrared, and mid-infrared ranges.<sup>46,47</sup> To date, terahertz FEL of the facility is the most powerful source of coherent narrowband radiation in the world in the spectral range of 25–111  $\text{cm}^{-1}$  (90–400  $\mu\text{m}$ ; 0.75–3.3 THz). The unique radiation parameters, including an average radiation power of 0.5 kW and a peak power of about 1 MW, are provided using an energy recovery linear accelerator for electron acceleration and a resonator-type FEL. In all experiments, the NovoFEL facility was operated in the macropulse lasing mode.<sup>48</sup> This regime allows for the use of macropulses of radiation with a minimum duration determined by the optical resonator of the THz FEL. The minimum reliable duration of the macropulse when using the range of 0.75–3.3 THz is 50–100  $\mu\text{s}$ . In all experiments, macropulses of 60  $\mu\text{s}$  duration were used.

The magnetization dynamics of paramagnetic species has been investigated using monochromatic radiation from the NovoFEL with 76.9  $\text{cm}^{-1}$  (130  $\mu\text{m}$ ; 2.31 THz) wavenumber. The repetition rate

was 1–5 Hz and was limited by the thermal relaxation time of the studied systems, which is in the range of 10–100 ms. The average radiation power was measured using a Gentec-EO UP19K-15S-VR detector (Gentec-EO, Quebec, QC, Canada) and was in the range of 2–25 W. The average power was measured in front of the THz waveguide, so the actual power reaching the sample was at least half as high.<sup>49</sup> A detailed description of the THz beamline of the endstation is given elsewhere.<sup>50–52</sup> The typical radiation spectrum is shown in Figs. S1–S2 of the [supplementary material](#). The choice of the exact wavenumber is driven by the most stable lasing of the NovoFEL including the achievable average power.

## B. Induction probehead

The conceptual detection circuit comprises a coil with a sample inserted in it, located in a static magnetic field. Throughout the relaxation process of the sample, changes in magnetic flux within the coil lead to the generation of an induced electromotive force (EMF). The detection of EMF occurs at the output of a coaxial cable connected to the coil. To theoretically assess the potential signal, registered in such a circuit, a numerical simulation was performed using the Elmer software.<sup>53</sup> The simulation employed a cylindrical pellet with a diameter of 4 mm and a thickness of 5 mm, containing a sample of one of the investigated compounds (see Sec. II B) diluted

with polyethylene in a ratio of 0.05:0.95. This sample was positioned inside an 80-turn coil of the same size, placed in a static magnetic field of 510 mT. The analysis was carried out at two initial sample temperatures of 3.4 and 8.0 K. More details are given in Sec. S3 of the [supplementary material](#). Considering the application of a low noise preamplifier (see Sec. II C) with a gain of 200, the estimated value of the recorded signal is ~10–30 mV that indicates the feasibility of signal registration.

The general design of the induction probehead mimics a commercial X-band microwave resonator,<sup>54,55</sup> since the two essential components for investigating the T-jump induced magnetization, namely the magnet and cryostat (see Sec. II C), are parts of the X-band EPR spectrometer.<sup>50</sup> [Figure 1](#) shows the construction of the proposed probehead, which takes into account all the size restrictions imposed by the latter. The central parts of the probehead are two G10 fiberglass tubes with an outer diameter of 12 mm and an inner diameter of 8 mm. A multimodal hollow metal/dielectric THz waveguide **1** is placed in one of these tubes (hereafter, the numbers correspond to [Fig. 1](#)). The waveguide is described elsewhere.<sup>49</sup> Another G10 tube holds a sample holder with a semi-rigid 0.086 in. microwave coaxial cable **2** inside that terminates with the detection coil **12**. The sample rod and the detection coil are easily extracted from the probehead, providing a quick sample exchange procedure, even when the cryostat is stabilized at helium temperatures.

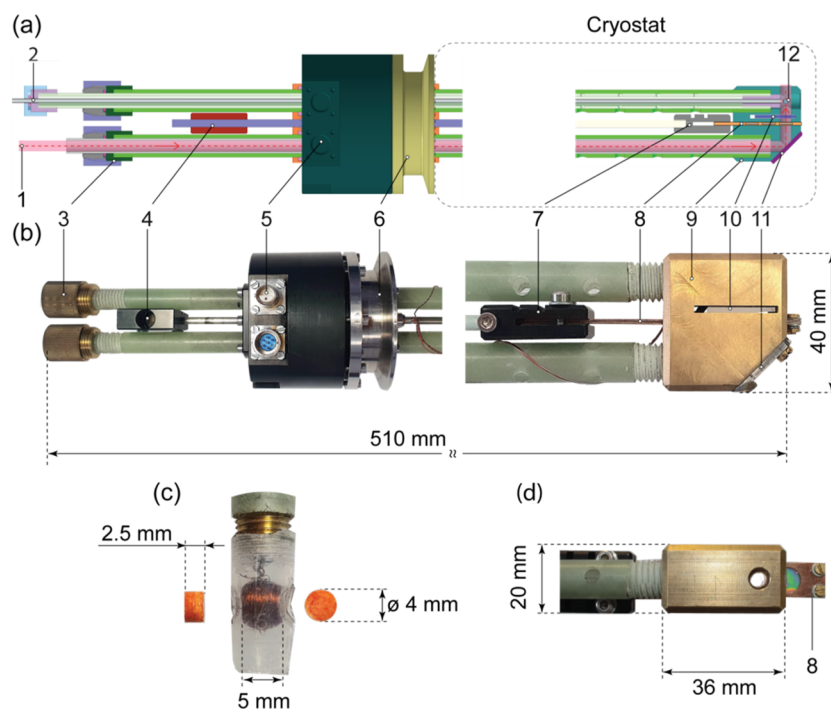


**FIG. 1.** Structure of the constructed induction probehead. (a) 2D view with a local sectional view of fiberglass tubes and depiction of the THz beam path. (b) Photographs of the probehead. The top and bottom parts are given in different scales for convenience. The bottom part is located inside the cryostat. (c) Photograph of the detection coil with a sample pellet. (d) A side view of the brass parallelepiped **9** with a plain mirror **11** and a polarizer holder **8**. The numbers show: (1) THz beam path, (2) microwave coaxial cable, (3) sealing chuck with silicone o-rings and polytetrafluoroethylene collet inside, (4) pusher, (5) cylinder made of anodized alloy D16 with several panel connectors, (6) vacuum KF-50 flange, (7) polarizer holder clamp, (8) polarizer holder, (9) brass parallelepiped with several functional holes, (10) quarter-wave plate, (11) stainless steel plane mirror, and (12) sample position.

The fiberglass tubes pass through a cylinder **5** made of anodized alloy D16 with several holes for various panel connectors, such as twin BNC for thermocouple wire and others. The cylinder **5** is connected to a vacuum KF-50 flange **6**, which isolates the lower part of the probehead, placed in the cryostat, from the upper part. The G10 tubes are screwed into a brass parallelepiped **9** with a size of  $20 \times 40 \times 36 \text{ mm}^3$  and several functional holes. A mirror **11** made of a polished stainless steel plate is fixed to **9** with four screws. The mirror turns the THz beam so that it passes through the polypropylene polarizer (Tydex, Saint Petersburg, Russia) and quarter-wave plate for single operation wavelength **10** (Tydex, Saint Petersburg, Russia) and finally reaches the sample, placed in the detection coil **12**. This mutual arrangement of the radiation propagation vector  $\mathbf{k}$  and the static magnetic field  $B_0$  corresponds to the Faraday geometry and allows for selective excitation of inter-Kramers doublet transitions of suitable high-spin objects.<sup>56</sup> The polarizer is placed in one of the three slots of the holder **8**. Another polarizer rotated at an angle of  $90^\circ$  with respect to the first one is placed in its other slot, and the last slot is empty. The clamp **7** is connected to the pusher **4** with a two-piece rod made of stainless steel and fiberglass to prevent thermal coupling. By moving the pusher **4** back and forth, one of two circular polarizations of the incident THz radiation can be selected or the polarizer can be omitted during the experiment without removing the probehead from the cryostat.

A close view of the detection coil is shown in Fig. 1(c). The coil consists of 80 turns of 0.09 mm diameter heat-resistant enameled copper wound on a polypropylene tube and soldered to the coaxial cable. The coil and transmission line have the following  $L$ ,  $R$ , and  $C$  values:  $146 \mu\text{H}$ ,  $9.1 \Omega$ , and  $17 \text{ nF}$ , respectively, measured at 100 kHz at room temperature using an MS5308 LCR meter (Mastech, Charlotte, NC, USA). A protective cover made of an Eppendorf safe-lock tube (Eppendorf, Enfield, CT, USA) is provided to reinforce the coil and prevent its possible displacement. The sample is a compressed pellet of a mixture of investigated compound and polyethylene (see Sec. II D), 4 mm in diameter and 1–4 mm thick. The pellet fits tightly into the tube and is held securely by friction. To ensure that the entire system is sealed, a chuck with silicone o-rings **3** is provided to hold both the main G10 tubes and other internal tubes.

### C. Experimental setup

The magnetization dynamics of several model paramagnetic compounds (see Sec. II D) induced by pulsed heating was investigated at the EPR endstation of the NovoFEL facility.<sup>50,51</sup> Figure 2 shows the general scheme of the experimental setup. In detail, the sample pellet is placed inside the induction coil (see Sec. II B) located at the end of the sample holder (see Fig. 1). The sample holder is inserted in the helium cryostat placed between the poles of the electromagnet, which allows for using a magnetic field in the range of 0–900 mT. The magnetic field is controlled using a homemade magnetic field controller<sup>57</sup> and is supplied by a homemade power supply. The magnetic field stability is better than  $10 \mu\text{T h}^{-1}$ . The signal from the coil is amplified using a low noise preamplifier SR560 (Stanford Research Systems, Sunnyvale, CA, USA) with 1 MHz bandwidth and a gain of 200 and detected using a 100 MHz Keysight DSO-X 2012A (Keysight Technologies, Santa Rosa, CA, USA). The arbitrary

waveform generator of the same oscilloscope was used to trigger the electronic modulation system of the NovoFEL that generated THz macropulses. The shape and intensities of the macropulses were tracked in parallel with the experiment.<sup>52</sup> The temperature of the helium cryostat (Cryotrade Engineering, Moscow, Russia) was controlled using a LakeShore 335 temperature controller (Lake Shore Cryotronics, Westerville, OH, USA) equipped with a Cernox cryogenic temperature sensor and type E thermocouple (both Lake Shore Cryotronics, Westerville, OH, USA). All experiments were carried out in the temperature range of 3.4–8.0 K. The temperature stability was better than 0.05 K. The measurements were fully automated using the open-source software Atomize.<sup>58</sup> The measurements of the temporal dynamics of magnetization were repeated several times at the same  $T_0$  or  $B_0$  for the same pellet to perform statistical analysis of the obtained data. This approach does not take into account uncertainties in the sample preparation and arrangement, but at least includes instabilities of the cryostat temperature, THz macropulse power, least square fitting errors, and other instrumental factors.

### D. Model compounds

To study the temporal dynamics of the magnetization induced by the T-jump, three compounds were used, namely [VO(TPP)], where TPP is 5,10,15,20-tetraphenylporphyrin; [CoTp<sub>2</sub>], where Tp is bis[tris(pyrazolyl)borate]; and [Dy(HL)(L)(MeOH)<sub>2</sub>]-2MeOH, where H<sub>2</sub>L is *N'*-(3,5-di-*tert*-butyl-2-hydroxybenzylidene)isonicotinohydrazide. The chemical structures of the compounds are shown in Fig. 3. Hereinafter, the chemical abbreviations [VO(TPP)], [CoTp<sub>2</sub>], and [Dy(HL)(L)(MeOH)<sub>2</sub>] (two methanol molecules in the outer sphere of the complex are omitted for clarity) will be used for them. All compounds have different magnetic moments that are determined by total electron spin  $S$  for [VO(TPP)] ( $S = 1/2$ ) and [CoTp<sub>2</sub>] ( $S = 3/2$ ) within the approximation of the spin Hamiltonian. This approximation is not completely satisfied for [CoTp<sub>2</sub>];<sup>59</sup> nevertheless, for simplicity, the value of  $S$  is used to mark the magnetic moment of this compound. Paramagnetic lanthanides have a large unquenched orbital momentum associated with high magnetic anisotropy and require the use of the total angular momentum  $J$ . In the case of [Dy(HL)(L)(MeOH)<sub>2</sub>],  $J$  is equal to 15/2. The synthesis as well as the characterization of the magnetic properties of [VO(TPP)] and [CoTp<sub>2</sub>] have been described elsewhere.<sup>59–62</sup> Due to the existence of two crystal forms of [CoTp<sub>2</sub>] (monoclinic and tetragonal),<sup>62</sup> additional AC magnetic measurements were carried out using exactly the sample pellet used to investigate the T-jump induced magnetization dynamics. The details are given in Sec. S4 of the supplementary material. The synthesis, characterization of [Dy(HL)(L)(MeOH)<sub>2</sub>], as well as the results of DC and AC magnetic measurements are given in Sec. S5 of the supplementary material.

The studied compounds were finely ground, mixed with ultra-high molecular weight polyethylene powder (Micro Powders, Tarrytown, NY, USA), and pressed into pellets with a diameter of 4 mm. The pellet contains the following amount of paramagnetic species: 2.7 mg of [VO(TPP)], 1.5 mg of [CoTp<sub>2</sub>], and 3.1 mg of [Dy(HL)(L)(MeOH)<sub>2</sub>]. The transparency of the pellets at the used wavenumber of  $76.9 \text{ cm}^{-1}$  ( $130 \mu\text{m}$ ; 2.31 THz) is about 20%–40%



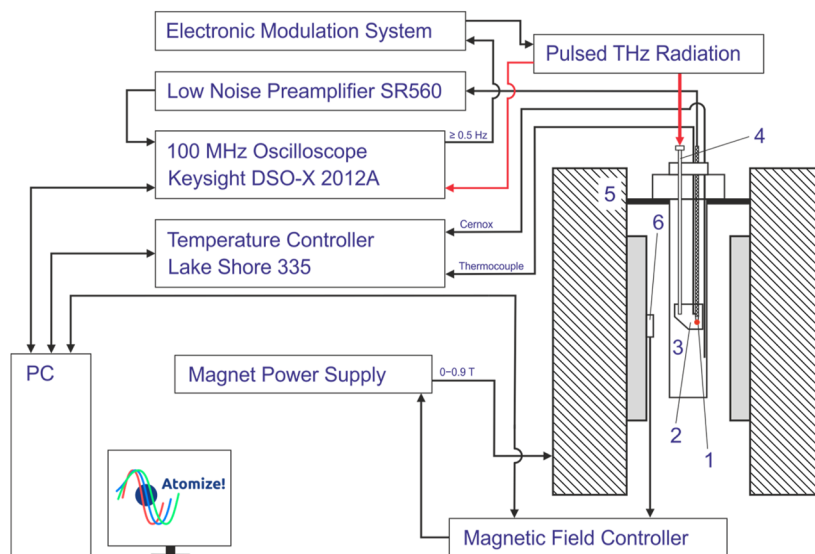


**FIG. 2.** (a) General scheme of the experimental setup for measuring the temporal dynamics of magnetization induced by pulsed THz radiation. The numbers show: (1) polyethylene sample pellet with a length of 1–4 mm and a diameter of 4 mm, (2) parallelepiped with the plain mirror, polarized holder, and quarter-wave plate slot, (3) helium cryostat, (4) THz waveguide,<sup>49</sup> (5) electromagnet, and (6) Hall probe.

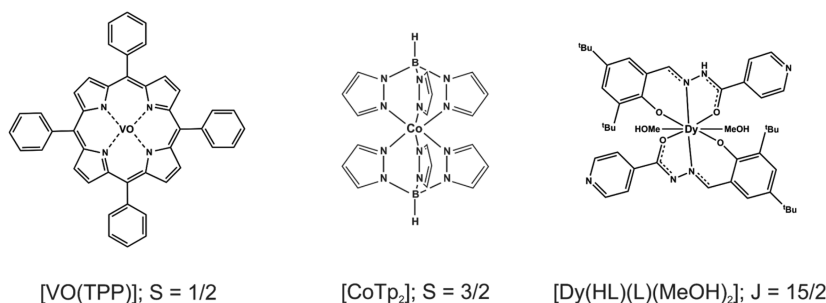


**FIG. 3.** Structures of the compounds used in this work, namely,  $[\text{VO}(\text{TPP})]$ , where TPP is 5,10,15,20-tetraphenylporphyrin;  $[\text{CoTp}_2]$ , where Tp is bis[tris(pyrazolyl)borate]; and  $[\text{Dy}(\text{HL})(\text{L})(\text{MeOH})_2] \cdot 2\text{MeOH}$ , where  $\text{H}_2\text{L}$  is  $N'$ -(3,5-di-tert-butyl-2-hydroxy-benzylidene)isonicotinohydrazide.

as controlled by far-infrared Fourier transform infrared (FTIR) spectra.

### III. THEORETICAL MODEL

Consider a paramagnetic system in thermal equilibrium with the lattice, placed in an external static magnetic field. Under a perturbation, such as a sudden change in magnetic field or lattice temperature, the  $z$ -component of the magnetization  $M$  reverts to its equilibrium value  $M_{eq}$  with a time constant called the longitudinal or spin–lattice relaxation time,  $T_1$ .<sup>63</sup> The relaxation time measured in AC magnetometry is commonly referred to as  $\tau$ . This is essentially an approximation when a single relaxation time is used to describe a multilevel high-spin system, in which there is a different  $T_1$  for each transition. The comparison between these times is not straightforward.<sup>64,65</sup> Since the proposed inductive detection is not a resonant method, hereinafter we used a symbol  $\tau$  to describe

the relaxation time and referred to it as either the longitudinal or spin–lattice relaxation time. The final expression for the recovery of  $M_z$  in the notation used is given by the following equation:

$$M(t) = M_{eq} - (M_{eq} - M_0) \cdot \exp(-t/\tau), \quad (1)$$

where  $M_0$  is the magnetization value before the perturbation. The value of  $M_{eq}$  in the high-temperature limit,  $g\beta B_0 S/kT \ll 1$ , is linearly dependent on the external magnetic field and is inversely proportional to temperature, as shown in the following equation:<sup>63</sup>

$$M_{eq} = -g\beta N_0 \frac{\sum_{m=-S}^S m \cdot \exp\left(-\frac{g\beta B_0 m}{kT}\right)}{\sum_{m=-S}^S \exp\left(-\frac{g\beta B_0 m}{kT}\right)} \approx N_0 \frac{g^2 \beta^2 B_0 S(S+1)}{3kT} = C \frac{B_0}{T}, \quad (2)$$

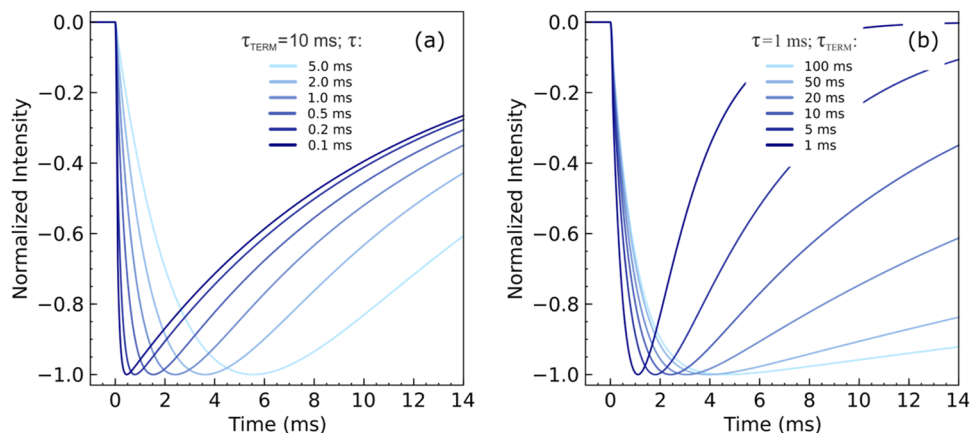


**FIG. 4.** Numerical calculation of the temporal dynamics of the magnetization induced by the T-jump (a) at a constant thermal relaxation time  $\tau_{TERM}$  of 10 ms and different relaxation times  $\tau$  from 0.1 to 5.0 ms (see the legend) and (b) at a constant relaxation time  $\tau$  of 1 ms and different thermal relaxation times  $\tau_{TERM}$  from 1 to 100 ms (see the legend). A fixed initial temperature of 4.0 K, a pulse duration of 100  $\mu$ s, and  $\alpha$  of 0.1 K were used.

where  $N_0$  is the total number of paramagnetic species,  $\beta$  is the Bohr magneton,  $g$  is the electron  $g$ -factor of the paramagnetic species,  $k$  is the Boltzmann constant,  $S$  is the total electron spin,  $B_0$  is the value of the static magnetic field,  $T$  is the temperature of the paramagnetic system, and  $C$  is a constant determined by the properties of the system. For  $B_0$  and  $T$  (see Sec. II C) used in this work, the high-temperature limit is always satisfied. Then, since the temperature jump was used as the perturbation, the magnetization dynamics can be written as given in the following equation:

$$M(t) = C \frac{B_0}{T(t)} - \left( C \frac{B_0}{T(t)} - C \frac{B_0}{T_0} \right) \cdot \exp(-t/\tau), \quad (3)$$

where  $t = 0$  corresponds to the beginning of the perturbation, which in our case is determined by the THz macropulse (see Sec. II A), and  $T_0$  is equal to the cryostat temperature (see Sec. II C).

The temperature dynamics of the sample is given by Eq. (4). It consists of two parts: (i) fast linear heating caused by the THz macropulse during the time  $0 \leq t \leq t_p$ , where  $t_p$  is the duration of the macropulse; and (ii) thermal relaxation with a characteristic time  $\tau_{TERM}$  that is also present during the macropulse. The heating rate is determined by an empirical parameter  $\alpha$  that depends on the macropulse power and the heat capacity of the sample. Such a model corresponds to the simplest case of uniform heating of the sample with heat capacity and thermal relaxation time that are independent of temperature,

$$T(t) = \begin{cases} T_0 + \frac{\alpha t}{t_p} \cdot \exp(-t/\tau_{TERM}), & 0 \leq t \leq t_p, \\ T_0 + \alpha \cdot \exp(-t/\tau_{TERM}), & t > t_p. \end{cases} \quad (4)$$

The relaxation time  $\tau$  in Eq. (3) is also assumed to be independent of  $T$ . This approximation is valid in most cases when there are no phase transitions in the studied compounds, and the temperature dependence of the relaxation time does not change significantly upon a temperature increase of a few percent. In the limit of an

infinitesimal temperature jump, the obtained  $\tau$  approaches the value corresponding to the temperature  $T_0$ . In other cases, the model described gives an average value of  $\tau$  for the range of temperatures defined by the T-jump.

Figure 4 shows the results of numerical calculation of the temporal dynamics of the T-jump induced magnetization for different values of  $\tau$  or  $\tau_{TERM}$  at  $\alpha$  corresponding to a T-jump of about 1 K,  $t_p$ , and  $T_0$  corresponding to typical experimental values. Both the longitudinal and thermal relaxation times affect the leading and trailing edges of the magnetization dynamics, where  $\tau$  mainly determines the front edge and  $\tau_{TERM}$  determines the trailing one. Usually,  $\tau_{TERM} \gg \tau$ , so the thermal relaxation time can be determined from the trailing edge. As for the longitudinal relaxation time, qualitatively, the longer the  $\tau$ , the greater the deviation of the front edge from the assumed linear rise in the sample temperature. It means that the spin system relaxes slowly; its temperature is lagging and does not coincide with the lattice temperature. Since the macropulse duration cannot be infinitesimal (see Sec. II A), the lower bound of the  $\tau$  value that can be determined by the proposed method is at least a few  $t_p$ .

The induction probehead proposed in this paper (see Sec. II B) is sensitive to the change in magnetic flux through the coil, so the recorded signal is proportional to the derivative of the sample magnetization. Figure 5 shows typical examples of the experimental EMF signals. It distinguishes two limiting cases of a sufficiently long and short  $\tau$ . After an initial sharp negative signal during the time  $t_p$ , the two cases differ in their subsequent dynamics that is determined by  $\tau$  and slowed down for the case of slow longitudinal relaxation. The trailing edge discussed earlier manifests itself as a long-lasting and low-intensity positive signal that is usually not measured until complete decay. For further analysis (see Secs. IV A and IV B), the raw experimental signal is integrated in the Julia programming language.<sup>66</sup> The examples of integrated signals are shown in the inset of Fig. 5. To extract  $\tau$  and  $\tau_{TERM}$ , the obtained kinetics is fitted by the least squares method using the LsqFit package with Eq. (3) as a model with fixed  $t_p$ ,  $\alpha$ , and  $T_0$ . The value of  $t_p$  is equal to the dura-

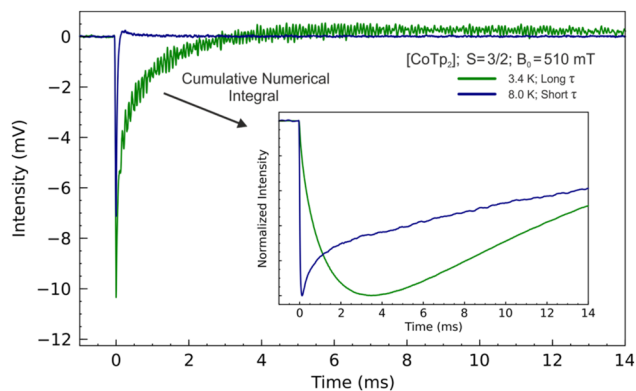


**FIG. 5.** Example of the experimental EMF signals for two limiting cases, a sufficiently long (dark green; [CoTp<sub>2</sub>] at 510 mT and 3.4 K) and a sufficiently short (dark blue; [CoTp<sub>2</sub>] at 510 mT and 8.0 K) relaxation time  $\tau$ . The signals were recorded using a low-noise preamplifier (see Sec. II C) with a gain of 200. The inset shows the cumulative integral of the raw experimental data. The integral shows the temporal dynamics of the T-jump induced magnetization.

tion of the THz macropulse used in the experiment. The fixed value of  $\alpha$  determines a T-jump and is about 1 K, which is a reasonable estimation under the experimental conditions used. The value of  $T_0$  is equal to the cryostat temperature (see also Sec. II C). A typical fit example is shown in Fig. S18 of the [supplementary material](#). The values of  $\tau_{TERM}$  and its dependence on temperature and magnetic field are not considered in this paper.

## IV. RESULTS AND DISCUSSION

### A. Qualitative description of the temperature-induced magnetization dynamics

#### 1. [VO(TPP)]

The first investigated system [VO(TPP)] has a low magnetic moment determined by  $S = 1/2$ . The response of the used sample pellet to an abrupt temperature change produces in the induction probehead a signal in the range of 1–10 mV at helium temperatures. This signal level corresponds to the use of the low noise preamplifier with a gain of 200 (see Sec. II C) and a typical THz macropulse duration and power, i.e., 60  $\mu$ s and 10 W. Such values are sufficient for reliable signal registration and subsequent determination of parameters  $\tau$  and  $\tau_{TERM}$  according to the previously proposed model. As for other high-spin systems utilized in this work, a higher response can be expected, allowing for the use of either shorter or less powerful THz pulses. According to Fig. 6, the relaxation time  $\tau$  of [VO(TPP)] determined by the front edge of the measured kinetics is comparable with the duration of the THz macropulse used. For example, the fit shows that  $\tau$  is in the range of 100–400  $\mu$ s at a temperature of 3.4 K in the magnetic field range of 110–680 mT. At a higher temperature,  $\tau$  is even shorter. Despite this, we decided to use this compound because of its profound characterization in the literature<sup>61</sup> and limited ourselves to a qualitative discussion.

According to Fig. 6(a), the dependence of  $\tau$  on the magnetic field is consistent with that commonly observed for this vanadyl por-

phyrin system.<sup>61</sup> Namely, in the investigated magnetic field range of up to 680 mT, the spin–lattice relaxation time grows with  $B_0$ . Various spin–spin and spin–nucleus interactions, which induce spin relaxation by breaking the time-reversal symmetry of the Kramers doublet,<sup>67,68</sup> are suppressed by the increase in the magnetic field, leading to an increase in  $\tau$ .

The temporal dynamics of the T-jump induced magnetization of [VO(TPP)] measured at different  $T_0$  is presented in Fig. 6(b). As it follows from the apparent shortening of the front edge of the kinetics, the  $\tau$  value of [VO(TPP)] expectedly decreases with increasing temperature. As it is already mentioned, it is not possible to correctly establish and analyze the exact relationship, due to unsuitable relaxation times that are comparable to  $t_p$ . Nevertheless, a comparison of  $\tau$  obtained using Eq. (3) with the results of AC magnetic measurements given in Ref. 61 allows us to estimate the magnitude of the T-jump as 1–2 K at the used parameters of THz radiation. Given the absolute signal amplitude for this system at 3.4 K (about 3 mV at 110 mT and 8 mV at 680 mT after the preamplifier with a gain of 200), such a T-jump is the lowest reasonable for a  $S = 1/2$  system with  $\sim 2.7$  mg of the paramagnet in the pellet.

#### 2. [Dy(HL)(L)(MeOH)<sub>2</sub>]

The dysprosium complex [Dy(HL)(L)(MeOH)<sub>2</sub>] with  $J = 15/2$  was used as an example of a system with a high magnetic moment. The preliminary magnetic characterization given in Sec. S5 of the [supplementary material](#) shows that this compound has a rather short spin–lattice relaxation time, which is only 550  $\mu$ s at a temperature of 3.0 K in an external magnetic field of 100 mT. This temporal dynamics of magnetization is very fast compared to other Dy<sup>3+</sup> complexes<sup>44,45,69–72</sup> and can hardly be studied quantitatively when induced by THz macropulses of 50–100  $\mu$ s duration. There is another feature for [Dy(HL)(L)(MeOH)<sub>2</sub>]. The out-of-phase component of the magnetic susceptibility  $\chi''$  agrees substantially better with the generalized Debye model under the assumption of two merged peaks in the dependence of  $\chi''$  on the frequency of the AC magnetic field (see Sec. S5 of the [supplementary material](#)). This assumes the existence of two parallel processes of magnetic relaxation that can be explained by the disorder of the *t*-butyl group of the ligand. Such a complex spin–lattice relaxation cannot be described by the simple model presented in Eq. (3), so only a qualitative description of the temperature-induced magnetization dynamics for [Dy(HL)(L)(MeOH)<sub>2</sub>] is possible.

As shown in Fig. 7(a), the magnitude of  $\tau$ , determined by the front edge of the measured kinetics, has a non-monotonic dependence on the magnetic field with the longest  $\tau$  for  $B_0$  in the range of 100–300 mT. This magnetic field range agrees well with the results of AC magnetic measurements. The general behavior of  $\tau$  on  $B_0$  corresponds to a significant influence of quantum tunneling of the magnetization on spin–lattice relaxation along with other typical relaxation mechanisms.

The Kramers ground state doublet of the dysprosium complex has the high projection ( $\pm 15/2$ ) of the total angular momentum that substantially increases the signal amplitude. The signal reaches about 18 mV at 100 mT and 90 mV at 3.4 K for 3.1 mg of the paramagnet in the pellet after the preamplifier with a gain of 200. The temperature dependence of  $\tau$  in the static magnetic field of 100 mT is shown in Fig. 7(b). The longest spin–lattice relaxation time obtained by fitting the experimental kinetics at 3.3 K and 100 mT is only



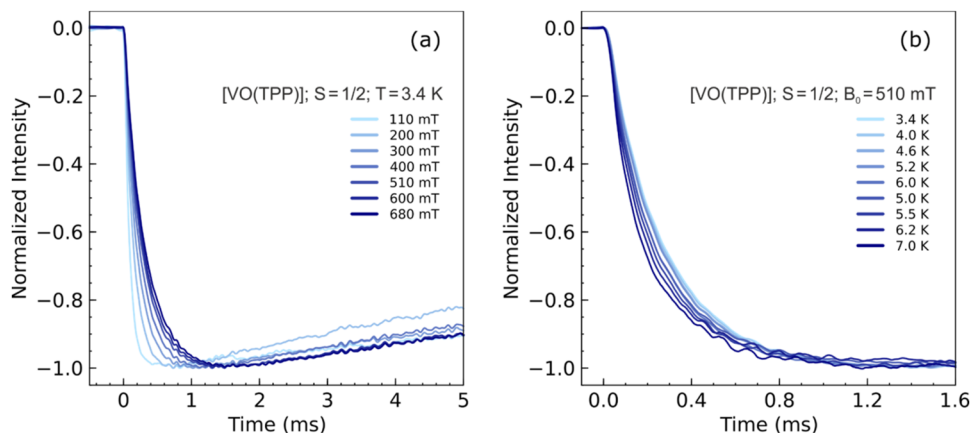


**FIG. 6.** Temporal dynamics of the T-jump induced magnetization of [VO(TPP)], measured with the induction probehead, (a) at a constant cryostat temperature of 3.4 K and different magnetic fields from 110 to 680 mT (see the legend) and (b) at a constant magnetic field of 510 mT and different cryostat temperatures from 3.4 to 7.0 K (see the legend). In all experiments, pulsed THz radiation with a wavenumber of  $76.9\text{ cm}^{-1}$  ( $130\text{ }\mu\text{m}$ ; 2.31 THz), a repetition rate of 3.7 Hz, and a pulse duration of  $60\text{ }\mu\text{s}$  was used. The average power measured in front of the THz waveguide was 11 W.

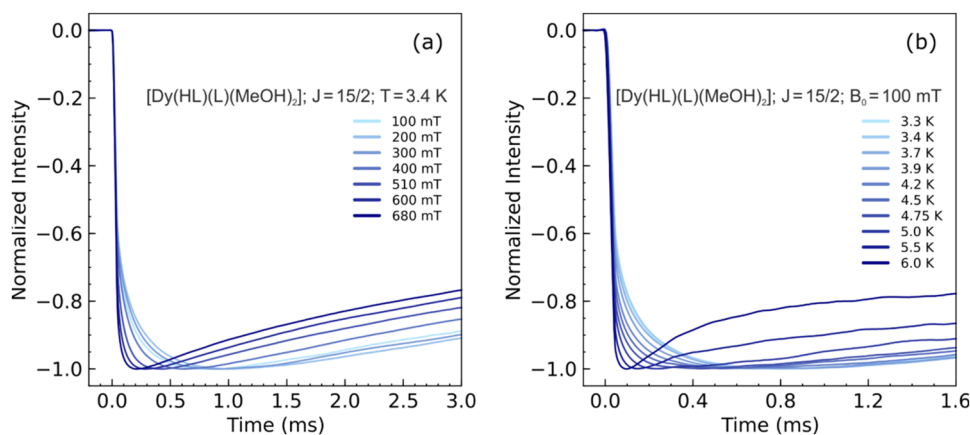


**FIG. 7.** Temporal dynamics of the T-jump induced magnetization of [Dy(HL)(L)(MeOH)<sub>2</sub>], measured with the induction probehead, (a) at a constant cryostat temperature of 3.4 K and different magnetic fields from 100 to 680 mT (see the legend) and (b) at a constant magnetic field of 100 mT and different cryostat temperatures from 3.3 to 6.0 K (see the legend). In all experiments, pulsed THz radiation with a wavenumber of  $76.9\text{ cm}^{-1}$  ( $130\text{ }\mu\text{m}$ ; 2.31 THz), a repetition rate of 3.1 Hz, and a pulse duration of  $60\text{ }\mu\text{s}$  was used. The average power measured in front of the THz waveguide was 1.9 W.

150  $\mu\text{s}$ . It is only twice the duration of the THz macropulses used, and, as a consequence, this estimation is probably inaccurate. If we compare this value with the AC magnetometry data, then the THz macropulse causes the T-jump of about 1–1.5 K, which is close to the case of [VO(TPP)] and [CoTp<sub>2</sub>]. It should also be noted that the quality of the fitting of experimental data using a single  $\tau$  by Eq. (3) is rather poor. One example is given in Sec. S6 of the [supplementary material](#). This indirectly confirms the proposed two parallel processes of magnetic relaxation in the processing of the AC magnetometry data. Additional information concerning the temperature dependence of  $\tau$  obtained by AC magnetic measurements is given in Sec. S5 of the [supplementary material](#).

## B. Quantitative description of the temperature-induced magnetization dynamics

### 1. [CoTp<sub>2</sub>]

The last example is a high-spin Co(II) complex [CoTp<sub>2</sub>] with  $S = 3/2$  within the approximation of the spin Hamiltonian. The electronic structure<sup>59</sup> and magnetic properties<sup>62</sup> of this compound have been described in detail in the literature. The magnitude of  $\tau$  in the temperature range of 3–10 K and  $B_0$  of up to 1 T is in the range of 10  $\mu\text{s}$ –100 ms. This makes [CoTp<sub>2</sub>] an ideal candidate to quantitatively describe the magnetization dynamics measured by the induction probehead if THz macropulses of about 100  $\mu\text{s}$

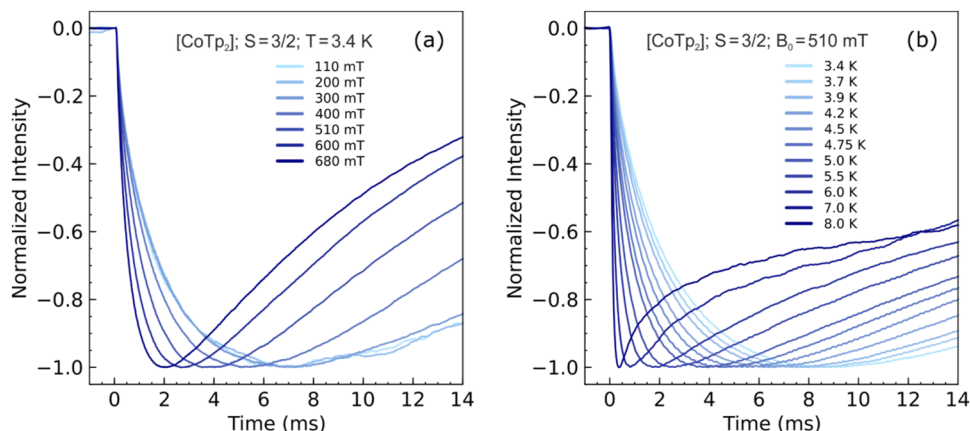


**FIG. 8.** Temporal dynamics of the T-jump induced magnetization of [CoTp<sub>2</sub>], measured with the induction probehead, (a) at a constant cryostat temperature of 3.4 K and different magnetic fields from 110 to 680 mT (see the legend) and (b) at a constant magnetic field of 510 mT and different cryostat temperatures from 3.4 to 8.0 K (see the legend). In all experiments, pulsed THz radiation with a wavenumber of 76.9 cm<sup>-1</sup> (130 μm; 2.31 THz), a repetition rate of 2.1 Hz, and a pulse duration of 60 μs was used. The average power measured in front of the THz waveguide was 12 W.

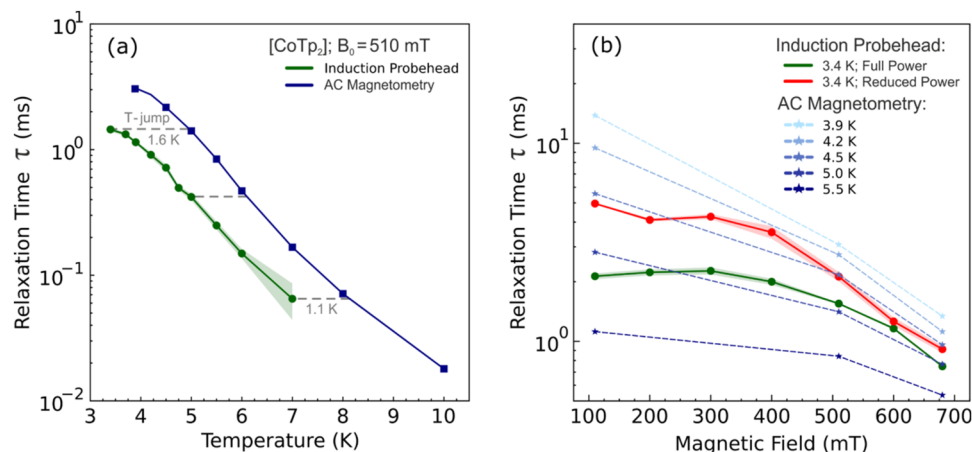
duration are used. Figure 8(a) shows the temporal dynamics of the T-jump induced magnetization measured at 3.4 K in different external magnetic fields in the range of 110–680 mT. Similar to the case of [Dy(HL)(L)(MeOH)<sub>2</sub>], there is an optimal  $B_0$  at which the most efficient suppression of quantum tunneling of the magnetization is observed. In this case, this value lies in the range of 0–110 mT, where measurements using an induction probehead were not performed due to the low signal intensity, which is proportional to  $B_0$ . The signal level was on the order of a few mV, see Fig. 5, for the [CoTp<sub>2</sub>] pellet investigated under THz macropulses of 60 μs duration and 12 W average power. Further decreasing the signal level and increasing the measurement time to obtain the required signal-to-noise ratio is not feasible. At higher magnetic fields, the spin–lattice relaxation time decreases significantly, reaching a value of  $750 \pm 20$  μs at 680 mT, which is consistent with AC magnetic measurements, taking into account T-jump (see also discussion below).

Figure 8(b) shows the temperature dependencies of the temporal dynamics of the magnetization measured at  $B_0$  of 510 mT. The fitting of the experimental data by Eq. (3) gives the  $\tau$  value lowering from  $1450 \pm 60$  μs at 3.4 K to  $65 \pm 21$  μs at 7.0 K. The standard deviation of  $\tau$  at 7.0 K reaches 33% that is mainly due to the significant drop in the signal intensity caused by (i) the increase in temperature and (ii) the decrease in the T-jump (see details below). Both of these reasons depend weakly on the nature of the sample, so the temperature of 7–8 K is the highest reasonable temperature at which the measurements can be made with the induction probehead in its current design.

A direct comparison of the obtained relaxation times at different temperatures and magnetic fields with AC magnetometry data is presented in Fig. 9. For better comparison, both sets of data were obtained using the same pellet. Both dependencies agree with each other, except for the T-jump that is inevitably present in the data measured by the induction probehead. According to Fig. 9(a), the T-jump value is close to 1.6 K at 3.4 K and further decreases to

1.1 K at 7.0 K. The temperatures indicated correspond to the cryostat temperature  $T_0$  in the measurement performed with the induction probehead. Strictly speaking, these T-jumps are smaller than the intrinsic T-jump, since  $\tau$  in Eq. (3) is independent of temperature. As a result, the fit yields an average  $\tau$  value for the temperature range defined by the intrinsic T-jump, while our estimates of the T-jumps here and in Sec. IV A correspond to the temperature difference between the AC magnetometry data at  $T_0$  and the average  $\tau$  obtained from the fit. The apparent decrease in the T-jump at higher  $T_0$  is related to the increase in the heat capacity of the sample.<sup>73</sup> Probably, T-jump can also influence the  $\tau_{TERM}$  value,<sup>50</sup> which is mainly determined by the macroscopic characteristics of the sample. Figure 9(b) shows a comparison of the magnetic field dependencies of  $\tau$  obtained using the induction probehead and AC magnetometry. Measurements with the induction probehead were carried out at 3.4 K, while the results of AC magnetometry are presented at different temperatures to visualize the T-jump. Two different techniques give consistent results taking into account the T-jump. Reducing the THz macropulse power by placing 1 mm thick polyethylene terephthalate films in the optical system of the endstation<sup>52</sup> decreases the T-jump predictably. Approximately 2.5 times reduction of the average power gives two times lower T-jump compared to the full power. Such a decrease in the T-jump inevitably leads to a worse signal-to-noise ratio, which can be clearly seen from the increase in the standard deviation of  $\tau$  values, presented by semi-transparent areas on the corresponding dependencies. Thus, reducing the magnitude of the T-jump to obtain a more accurate value of  $\tau$ , corresponding to the temperature  $T_0$ , is always a matter of finding a trade-off with the amplitude of the signal.

A separate case worth mentioning is the direct excitation of spin transitions by THz radiation with the wavenumber resonant with the energy splitting of levels within the spin system. Indeed, in addition to heating the sample with THz radiation and thus inducing magnetization dynamics, properly tuned THz radiation can cause direct transitions in the spin system of the studied com-



**FIG. 9.** Comparison of the relaxation times  $\tau$  of  $[\text{CoTp}_2]$ , obtained using the induction probehead and AC magnetic measurements, (a) at a constant magnetic field of 510 mT and different cryostat temperatures from 3.4 to 10 K and (b) at different magnetic fields in the range of 110–680 mT and a cryostat temperature of 3.4 K with full (12 W) or reduced (5.1 W) average power of pulsed THz radiation using the induction probehead. The cryostat temperature was in the range of 3.9–5.5 K (see the legend) in the case of AC magnetic measurements. The semi-transparent dark green and red areas show the standard deviation of the obtained values.

pounds.<sup>56</sup> Such transitions could result in a rapid change in the magnetization caused by the resonant THz macropulse and can be detected by the induction probehead. In the case of direct THz-induced spin transitions, the corresponding dynamics is expected to develop on the timescale of the THz macropulse, i.e., 50–100  $\mu\text{s}$ , allowing one to distinguish such a fast process from relatively slow spin–lattice and slow thermal relaxations. The detection of the resonant magnetization dynamics using the induction probehead has several apparent advantages compared to other experimental techniques. For example, it has superior temporal resolution compared to AC magnetometry and can detect EPR silent compounds in both magnetically concentrated and diluted forms.

## V. CONCLUSIONS

The proposed combination of the inductive detection with the creation of a nonequilibrium state by a sudden change in the lattice temperature caused by pulsed THz radiation demonstrates proper sensitivity and versatility. Virtually, any molecular spin system starting from a total spin  $S = 1/2$  can be investigated by the proposed method at temperatures of up to 8 K. For analyzing the measured temporal dynamics of the magnetization induced by T-jump, a simple model is proposed that allows for determining relaxation time  $\tau$  with a lower limit determined by the duration of the THz macropulses used, i.e., 50–100  $\mu\text{s}$ . The performed comprehensive analysis of magnetic relaxation data measured by the induction probehead and AC magnetometry shows good consistency at qualitative and quantitative levels for the investigated systems with different total spin or total angular momentum. This allows us to consider the proposed method, which has its advantages and limitations, as an alternative to other methods, such as AC magnetometry and pulsed EPR, for studying magnetization dynamics in molecular spin systems.

The apparent advantage of the proposed method compared to AC magnetometry is the rapid measurement time, even taking into account the lower sensitivity. In this case, there is no need to sweep the frequency of the AC magnetic field to obtain the relaxation time  $\tau$ . It is sufficient to register only one kinetic in a static magnetic field and temperature of interest. The magnitude of the T-jump determines the amplitude of the recorded signal but inevitably affects the measured values of the relaxation time  $\tau$ . Reducing the T-jump to obtain a more accurate value of  $\tau$  is always a trade-off with the signal amplitude. In the measurements performed, the lower boundary of the T-jump was estimated to be 1–2 K, which allowed reliable signal registration in magnetic fields of 100 mT and higher, using a standard preamplifier and an oscilloscope. The temporal resolution of the proposed inductive detection is limited not by fast internal transient processes in the pickup coil, but by the duration of the heating pulse, which should be short compared to the characteristic relaxation time of the system. In the case of the NovoFEL, the THz macropulse duration is typically 50–100  $\mu\text{s}$ , which determines the shortest relaxation time available for this study. A unique advantage of using the NovoFEL as a radiation source in T-jump experiments with inductive detection is the possibility to investigate spin resonance processes. If THz quanta correspond to the energies of spin transitions in high-spin systems, the excited spin transitions can redistribute the population of spin levels, which is detected by the induction probehead. The access to magnetic relaxation processes and THz-induced direct spin transitions provided by the induction probehead makes the proposed approach an efficient general tool for studying the dynamics of molecular spin systems.

## SUPPLEMENTARY MATERIAL

The [supplementary material](#) provides (i) radiation spectra and THz macropulse shapes, (ii) estimation of the signal magnitude

recorded by the induction probehead, (iii) AC magnetic measurements of  $[\text{CoTp}_2]$ , (iv) synthesis and magnetic properties of  $[\text{Dy}(\text{HL})(\text{L})(\text{MeOH})_2] \cdot 2\text{MeOH}$ , and (v) additional figures.

## ACKNOWLEDGMENTS

This work was funded by the Russian Science Foundation, Grant No. 22-13-00376. The FTIR spectra of the studied compounds were measured with the support of the Ministry of Science and Higher Education of the Russian Federation. The authors kindly thank Dr. F. Santanni and Professor R. Sessoli (Laboratory of Molecular Magnetism, University of Florence, Italy) for providing  $[\text{VO}(\text{TPP})]$  samples and for the helpful scientific discussion on the manuscript. A.R.M. is grateful to Maryasov A.G. for helpful discussions on total angular momentum and quenching of orbital momentum. The synthesis, IR spectroscopy, single crystal x-ray diffraction, and magnetochemical studies of  $[\text{Dy}(\text{HL})(\text{L})(\text{MeOH})_2]$  were supported by the Ministry of Science and Higher Education of the Russian Federation as part of the State Assignment of the Kurnakov Institute of General and Inorganic Chemistry of the RAS. The single crystal x-ray diffraction and magnetochemical studies of  $[\text{Dy}(\text{HL})(\text{L})(\text{MeOH})_2]$  were performed using the equipment of the JRC PMR IGIC RAS. The PXRD patterns of  $[\text{Dy}(\text{HL})(\text{L})(\text{MeOH})_2]$  were measured using the equipment of Center for molecular composition studies of INEOS RAS with the support of the Ministry of Science and Higher Education of the Russian Federation (Contract No. 075-00277-24-00).

## AUTHOR DECLARATIONS

### Conflict of Interest

The authors have no conflicts to disclose.

## Author Contributions

**Anatoly R. Melnikov:** Conceptualization (equal); Data curation (lead); Formal analysis (lead); Investigation (lead); Writing – original draft (lead); Writing – review & editing (equal). **Mikhail Yu. Ivanov:** Methodology (lead); Resources (equal); Writing – review & editing (equal). **Arkady A. Samsonenko:** Data curation (equal); Writing – review & editing (equal). **Yaroslav V. Getmanov:** Resources (equal). **Igor A. Nikovski:** Resources (equal). **Anna K. Matiukhina:** Resources (equal). **Ekaterina N. Zorina-Tikhonova:** Resources (equal); Writing – review & editing (equal). **Julia K. Voronina:** Resources (equal). **Alexander S. Goloveshkin:** Resources (equal). **Konstantin A. Babeshkin:** Resources (equal). **Nikolay N. Efimov:** Resources (equal); Writing – review & editing (equal). **Mikhail A. Kiskin:** Resources (equal). **Igor L. Eremanov:** Resources (equal); Supervision (equal). **Matvey V. Fedin:** Conceptualization (equal); Supervision (equal); Writing – review & editing (equal). **Sergey L. Veber:** Conceptualization (lead); Funding acquisition (lead); Supervision (equal); Writing – review & editing (lead).

## DATA AVAILABILITY

The raw data as well as the drawings of the induction probehead are available from the corresponding authors upon reasonable request.

## REFERENCES

- R. Sessoli, D. Gatteschi, A. Caneschi, and M. A. Novak, “Magnetic bistability in a metal-ion cluster,” *Nature* **365**(6442), 141–143 (1993).
- C. Sangregorio, T. Ohm, C. Paulsen, R. Sessoli, and D. Gatteschi, “Quantum tunneling of the magnetization in an iron cluster nanomagnet,” *Phys. Rev. Lett.* **78**(24), 4645–4648 (1997).
- N. Ishikawa, M. Sugita, and W. Wernsdorfer, “Quantum tunneling of magnetization in lanthanide single-molecule magnets: Bis(phthalocyaninato)terbium and bis(phthalocyaninato)dysprosium anions,” *Angew. Chem., Int. Ed.* **44**(19), 2931–2935 (2005).
- W. Wernsdorfer, “From micro- to nano-SQUIDS: Applications to nanomagnetism,” *Supercond. Sci. Technol.* **22**(6), 064013 (2009).
- M. Buchner, K. Höfler, B. Henne, V. Ney, and A. Ney, “Tutorial: Basic principles, limits of detection, and pitfalls of highly sensitive SQUID magnetometry for nanomagnetism and spintronics,” *J. Appl. Phys.* **124**(16), 161101 (2018).
- E. Moreno-Pineda and W. Wernsdorfer, “Measuring molecular magnets for quantum technologies,” *Nat. Rev. Phys.* **3**(9), 645–659 (2021).
- A.-L. Barra, A. Caneschi, A. Cornia, D. Gatteschi, L. Gorini, L.-P. Heiniger, R. Sessoli, and L. Sorace, “The origin of transverse anisotropy in axially symmetric single molecule magnets,” *J. Am. Chem. Soc.* **129**(35), 10754–10762 (2007).
- E. Moreno Pineda, N. F. Chilton, R. Marx, M. Dörfel, D. O. Sells, P. Neugebauer, S.-D. Jiang, D. Collison, J. van Slageren, E. J. L. McInnes, and R. E. P. Winpenny, “Direct measurement of dysprosium(III) · · · dysprosium(III) interactions in a single-molecule magnet,” *Nat. Commun.* **5**(1), 5243 (2014).
- K. Bader, M. Winkler, and J. van Slageren, “Tuning of molecular qubits: Very long coherence and spin–lattice relaxation times,” *Chem. Commun.* **52**(18), 3623–3626 (2016).
- M. Atzori, E. Morra, L. Tesi, A. Albino, M. Chiesa, L. Sorace, and R. Sessoli, “Quantum coherence times enhancement in vanadium(IV)-based potential molecular qubits: The key role of the vanadyl moiety,” *J. Am. Chem. Soc.* **138**(35), 11234–11244 (2016).
- C.-J. Yu, M. J. Graham, J. M. Zadrozny, J. Niklas, M. D. Krzyaniak, M. R. Wasielewski, O. G. Poluektov, and D. E. Freedman, “Long coherence times in nuclear spin-free vanadyl qubits,” *J. Am. Chem. Soc.* **138**(44), 14678–14685 (2016).
- M. J. Giansiracusa, E. Moreno-Pineda, R. Hussain, R. Marx, M. Martínez Prada, P. Neugebauer, S. Al-Badran, D. Collison, F. Tuna, J. van Slageren, S. Carretta, T. Guidi, E. J. L. McInnes, R. E. P. Winpenny, and N. F. Chilton, “Measurement of magnetic exchange in asymmetric lanthanide dimetallics: Toward a transferable theoretical framework,” *J. Am. Chem. Soc.* **140**(7), 2504–2513 (2018).
- S. Carretta, P. Santini, G. Amoretti, T. Guidi, J. R. D. Copley, Y. Qiu, R. Caciuffo, G. Timco, and R. E. P. Winpenny, “Quantum oscillations of the total spin in a heterometallic antiferromagnetic ring: Evidence from neutron spectroscopy,” *Phys. Rev. Lett.* **98**(16), 167401 (2007).
- E. Garlatti, A. Chiesa, T. Guidi, G. Amoretti, P. Santini, and S. Carretta, “Unravelling the spin dynamics of molecular nanomagnets with four-dimensional inelastic neutron scattering,” *Eur. J. Inorg. Chem.* **2019**(8), 1106–1118.
- E. Garlatti, L. Tesi, A. Lunghi, M. Atzori, D. J. Voneshen, P. Santini, S. Sanvito, T. Guidi, R. Sessoli, and S. Carretta, “Unveiling phonons in a molecular qubit with four-dimensional inelastic neutron scattering and density functional theory,” *Nat. Commun.* **11**(1), 1751 (2020).
- M. Mannini, F. Pineider, P. Sainctavit, C. Danielli, E. Otero, C. Sciancalepore, A. M. Talarico, M.-A. Arrio, A. Cornia, D. Gatteschi, and R. Sessoli, “Magnetic memory of a single-molecule quantum magnet wired to a gold surface,” *Nat. Mater.* **8**(3), 194–197 (2009).



- <sup>17</sup>M. Mannini, F. Pineider, C. Danieli, F. Totti, L. Sorace, P. Sainctavit, M.-A. Arrio, E. Otero, L. Joly, J. C. Cezar, A. Cornia, and R. Sessoli, "Quantum tunnelling of the magnetization in a monolayer of oriented single-molecule magnets," *Nature* **468**(7322), 417–421 (2010).
- <sup>18</sup>G. van der Laan and A. I. Figueroa, "X-ray magnetic circular dichroism—A versatile tool to study magnetism," *Coord. Chem. Rev.* **277–278**, 95–129 (2014).
- <sup>19</sup>C. Wäckerlin, F. Donati, A. Singha, R. Baltic, S. Rusponi, K. Diller, F. Patthey, M. Pivetta, Y. Lan, S. Klyatskaya, M. Ruben, H. Brune, and J. Dreiser, "Giant hysteresis of single-molecule magnets adsorbed on a nonmagnetic insulator," *Adv. Mater.* **28**(26), 5195–5199 (2016).
- <sup>20</sup>M. Studniarek, C. Wäckerlin, A. Singha, R. Baltic, K. Diller, F. Donati, S. Rusponi, H. Brune, Y. Lan, S. Klyatskaya, M. Ruben, A. P. Seitsonen, and J. Dreiser, "Understanding the superior stability of single-molecule magnets on an oxide film," *Adv. Sci.* **6**(22), 1901736 (2019).
- <sup>21</sup>P. Carretta and A. Lascialfari, *NMR-MRI,  $\mu$ SR and Mössbauer Spectroscopies in Molecular Magnets* (Springer, Milano, Milan, 2007).
- <sup>22</sup>A. Schweiger and R. R. Ernst, "Pulsed ESR with longitudinal detection. A novel recording technique," *J. Magn. Reson.* (1969) **77**(3), 512–523 (1988).
- <sup>23</sup>A. Borel, L. Helm, A. E. Merbach, V. A. Atsarkin, V. V. Demidov, B. M. Odintsov, R. L. Belford, and R. B. Clarkson, "T1e in four Gd<sup>3+</sup> chelates: LODEPR measurements and models for electron spin relaxation," *J. Phys. Chem. A* **106**(26), 6229–6231 (2002).
- <sup>24</sup>M. Bouterfas, S. Mouaziz, and R. S. Popovic, "14 GHz longitudinally detected electron spin resonance using microHall sensors," *J. Magn. Reson.* **282**, 47–53 (2017).
- <sup>25</sup>X. Tang, S. Suddarth, S. Kantesaria, and M. Garwood, "A frequency-swept, longitudinal detection EPR system for measuring short electron spin relaxation times at ultra-low fields," *J. Magn. Reson.* **342**, 107279 (2022).
- <sup>26</sup>M. Eigen and L. de Mayer, *Tech. Org. Chem. Part II* (Wiley: Interscience, New York, 1963).
- <sup>27</sup>H. Staerk and G. Czerlinski, "Nanosecond heating of aqueous systems by giant laser pulses," *Nature* **205**(4966), 63–64 (1965).
- <sup>28</sup>C. M. Phillips, Y. Mizutani, and R. M. Hochstrasser, "Ultrafast thermally induced unfolding of RNase A," *Proc. Natl. Acad. Sci. U. S. A.* **92**(16), 7292–7296 (1995).
- <sup>29</sup>J. Kubelka, "Time-resolved methods in biophysics. 9. Laser temperature-jump methods for investigating biomolecular dynamics," *Photochem. Photobiol. Sci.* **8**(4), 499–512 (2009).
- <sup>30</sup>E. G. Panarelli, P. Gast, and E. J. J. Groenen, "Temperature-cycle electron paramagnetic resonance," *Phys. Chem. Chem. Phys.* **22**(17), 9487–9493 (2020).
- <sup>31</sup>M. Sadqi, L. J. Lapidus, and V. Muñoz, "How fast is protein hydrophobic collapse?," *Proc. Natl. Acad. Sci. U. S. A.* **100**(21), 12117–12122 (2003).
- <sup>32</sup>G. Balakrishnan, Y. Hu, and T. G. Spiro, "Temperature-jump apparatus with Raman detection based on a solid-state tunable (1.80–2.05  $\mu$ m) kHz optical parametric oscillator laser," *Appl. Spectrosc.* **60**(4), 347–351 (2006).
- <sup>33</sup>J. F. Holzwarth, A. Schmidt, H. Wolff, and R. Volk, "Nanosecond temperature-jump technique with an iodine laser," *J. Phys. Chem.* **81**(24), 2300–2301 (1977).
- <sup>34</sup>J. S. Davis and W. F. Harrington, "Laser temperature-jump apparatus for the study of force changes in fibers," *Anal. Biochem.* **161**(2), 543–549 (1987).
- <sup>35</sup>J. J. Smith, J. A. McCray, M. G. Hibberd, and Y. E. Goldman, "Holmium laser temperature-jump apparatus for kinetic studies of muscle contraction," *Rev. Sci. Instrum.* **60**(2), 231–236 (1989).
- <sup>36</sup>J. V. Beitz, G. W. Flynn, D. H. Turner, and N. Sutin, "Stimulated Raman effect. A new source of laser temperature-jump heating," *J. Am. Chem. Soc.* **92**(13), 4130–4132 (1970).
- <sup>37</sup>K. Petukhov, S. Bahr, W. Wernsdorfer, A.-L. Barra, and V. Mosser, "Magnetization dynamics in the single-molecule magnet Fe<sub>8</sub> under pulsed microwave irradiation," *Phys. Rev. B* **75**(6), 064408 (2007).
- <sup>38</sup>S. V. Tumanov, A. R. Melnikov, N. A. Artiukhova, A. S. Bogomyakov, O. A. Shevchenko, Ya. V. Getmanov, V. I. Ovcharenko, M. V. Fedin, and S. L. Veber, "Temperature dynamics of magnetoactive compounds under terahertz irradiation: Characterization by an EPR study," *Russ. Chem. Bull.* **71**(7), 1378–1384 (2022).
- <sup>39</sup>J. M. Zadrozny, J. Niklas, O. G. Poluektov, and D. E. Freedman, "Multiple quantum coherences from hyperfine transitions in a vanadium(IV) complex," *J. Am. Chem. Soc.* **136**(45), 15841–15844 (2014).
- <sup>40</sup>J. M. Zadrozny, J. Niklas, O. G. Poluektov, and D. E. Freedman, "Millisecond coherence time in a tunable molecular electronic spin qubit," *ACS Cent. Sci.* **1**(9), 488–492 (2015).
- <sup>41</sup>M. Atzori, L. Tesi, E. Morra, M. Chiesa, L. Sorace, and R. Sessoli, "Room-temperature quantum coherence and Rabi oscillations in vanadyl phthalocyanine: Toward multifunctional molecular spin qubits," *J. Am. Chem. Soc.* **138**(7), 2154–2157 (2016).
- <sup>42</sup>M. Atzori, L. Tesi, S. Benci, A. Lunghi, R. Righini, A. Taschin, R. Torre, L. Sorace, and R. Sessoli, "Spin dynamics and low energy vibrations: Insights from vanadyl-based potential molecular qubits," *J. Am. Chem. Soc.* **139**(12), 4338–4341 (2017).
- <sup>43</sup>V. V. Novikov, A. A. Pavlov, Y. V. Nelyubina, M.-E. Boulon, O. A. Varzatskii, Y. Z. Voloshin, and R. E. P. Wippeny, "A trigonal prismatic mononuclear cobalt(II) complex showing single-molecule magnet behavior," *J. Am. Chem. Soc.* **137**(31), 9792–9795 (2015).
- <sup>44</sup>C. A. P. Goodwin, F. Ortu, D. Reta, N. F. Chilton, and D. P. Mills, "Molecular magnetic hysteresis at 60 kelvin in dysprosocenium," *Nature* **548**(7668), 439–442 (2017).
- <sup>45</sup>F.-S. Guo, B. M. Day, Y.-C. Chen, M.-L. Tong, A. Mansikkamäki, and R. A. Layfield, "Magnetic hysteresis up to 80 kelvin in a dysprosium metallocene single-molecule magnet," *Science* **362**(6421), 1400–1403 (2018).
- <sup>46</sup>O. A. Shevchenko, V. S. Arbutov, N. A. Vinokurov, P. D. Vobly, V. N. Volkov, Ya. V. Getmanov, Ya. I. Gorbachev, I. V. Davidyuk, O. I. Deychuly, E. N. Dementyev, B. A. Dovzhenko, B. A. Knyazev, E. I. Kolobanov, A. A. Kondakov, V. R. Kozak, E. V. Kozyrev, V. V. Kubarev, G. N. Kulipanov, E. A. Kuper, I. V. Kuptsov, G. Ya. Kurkin, S. A. Krutikhin, L. E. Medvedev, S. V. Motygin, V. K. Ovchar, V. N. Osipov, V. M. Petrov, A. M. Pilan, V. M. Popik, V. V. Repkov, T. V. Salikova, I. K. Sedlyarov, S. S. Serednyakov, A. N. Skrinisky, S. V. Tararyshkin, A. G. Tribendis, V. G. Tcheskidov, K. N. Chernov, and M. A. Scheglov, "The Novosibirsk free electron laser—Unique source of terahertz and infrared coherent radiation," *Phys. Procedia* **84**, 13–18 (2016).
- <sup>47</sup>G. N. Kulipanov, E. G. Bagryanskaya, E. N. Chesnokov, Y. Y. Choporova, V. V. Gerasimov, Y. V. Getmanov, S. L. Kiselev, B. A. Knyazev, V. V. Kubarev, S. E. Peltek, V. M. Popik, T. V. Salikova, M. A. Scheglov, S. S. Seredniakov, O. A. Shevchenko, A. N. Skrinisky, S. L. Veber, and N. A. Vinokurov, "Novosibirsk free electron laser—Facility description and recent experiments," *IEEE Trans. Terahertz Sci. Technol.* **5**(5), 798–809 (2015).
- <sup>48</sup>O. A. Shevchenko, A. R. Melnikov, S. V. Tararyshkin, Y. V. Getmanov, S. S. Serednyakov, E. V. Bykov, V. V. Kubarev, M. V. Fedin, and S. L. Veber, "Electronic modulation of THz radiation at NovoFEL: Technical aspects and possible applications," *Materials* **12**(19), 3063 (2019).
- <sup>49</sup>A. R. Melnikov, A. A. Samsonenko, Y. V. Getmanov, O. A. Shevchenko, D. A. Shevchenko, A. A. Stepanov, M. V. Fedin, M. A. Yurkin, and S. L. Veber, "Broadband multimodal THz waveguides for efficient transfer of high-power radiation in space-confined conditions," *Opt. Laser Technol.* **143**, 107375 (2021).
- <sup>50</sup>S. L. Veber, S. V. Tumanov, E. Yu. Fursova, O. A. Shevchenko, Y. V. Getmanov, M. A. Scheglov, V. V. Kubarev, D. A. Shevchenko, I. I. Gorbachev, T. V. Salikova, G. N. Kulipanov, V. I. Ovcharenko, and M. V. Fedin, "X-band EPR setup with THz light excitation of Novosibirsk Free Electron Laser: Goals, means, useful extras," *J. Magn. Reson.* **288**, 11–22 (2018).
- <sup>51</sup>A. R. Melnikov, M. A. Kiskin, Y. V. Getmanov, O. A. Shevchenko, M. V. Fedin, and S. L. Veber, "Technical and software improvements of the EPR spectroscopy endstation at the NovoFEL facility: Status 2020," *AIP Conf. Proc.* **2299**(1), 030010 (2020).
- <sup>52</sup>A. R. Melnikov, E. V. Kalneus, Y. V. Getmanov, D. A. Shevchenko, V. V. Gerasimov, O. A. Anisimov, M. V. Fedin, and S. L. Veber, "Comparative study of single crystal and polymeric pyroelectric detectors in the 0.9–2.0 THz range using monochromatic laser radiation of the NovoFEL," *Polymers* **15**(20), 4124 (2023).
- <sup>53</sup>M. Malinen and P. Råback, in *Multiscale Model. Methods Appl. Mater. Sci.*, edited by K. Ivan and G. Sutmann (Forschungszentrum Juelich, Jülich, 2013), pp. 101–113.
- <sup>54</sup>E. Gentsch and D. Schmalbein, US5345203A (6 September 1994).
- <sup>55</sup>E. Reijerse and A. Savitsky, *eMagRes* (John Wiley & Sons, Ltd., 2017), pp. 187–206.



- <sup>56</sup>A. G. Maryasov, M. K. Bowman, M. V. Fedin, and S. L. Veber, “Theoretical basis for switching a Kramers single molecular magnet by circularly-polarized radiation,” *Materials* **12**(23), 3865 (2019).
- <sup>57</sup>M. A. Bizin, N. P. Isaev, S. A. Baranov, A. R. Melnikov, and S. L. Veber, RU2799103C1 (4 July 2023).
- <sup>58</sup>See <https://github.com/Anatoly1010/Atomize> for more information about Atomize; accessed 22 March 2024.
- <sup>59</sup>A. A. Pavlov, J. Nehr Korn, Y. A. Pankratova, M. Ozerov, E. A. Mikhalyova, A. V. Polezhaev, Y. V. Nelyubina, and V. V. Novikov, “Detailed electronic structure of a high-spin cobalt(II) complex determined from NMR and THz-EPR spectroscopy,” *Phys. Chem. Chem. Phys.* **21**(16), 8201–8204 (2019).
- <sup>60</sup>S. Trofimenko, “Boron-pyrazole chemistry,” *J. Am. Chem. Soc.* **88**(8), 1842–1844 (1966).
- <sup>61</sup>T. Yamabayashi, M. Atzori, L. Tesi, G. Cosquer, F. Santanni, M.-E. Boulon, E. Morra, S. Benci, R. Torre, M. Chiesa, L. Sorace, R. Sessoli, and M. Yamashita, “Scaling up electronic spin qubits into a three-dimensional metal–organic framework,” *J. Am. Chem. Soc.* **140**(38), 12090–12101 (2018).
- <sup>62</sup>J. Zhang, J. Li, L. Yang, C. Yuan, Y.-Q. Zhang, and Y. Song, “Magnetic anisotropy from trigonal prismatic to trigonal antiprismatic Co(II) complexes: Experimental observation and theoretical prediction,” *Inorg. Chem.* **57**(7), 3903–3912 (2018).
- <sup>63</sup>P. Atkins, J. De Paula, and J. Keeler, *Atkins’ Physical Chemistry*, 11th ed. (Oxford University Press, 2017).
- <sup>64</sup>L. Tesi, A. Lunghi, M. Atzori, E. Lucaccini, L. Sorace, F. Totti, and R. Sessoli, “Giant spin–phonon bottleneck effects in evaporable vanadyl-based molecules with long spin coherence,” *Dalton Trans.* **45**(42), 16635–16643 (2016).
- <sup>65</sup>D. Aravena and E. Ruiz, “Spin dynamics in single-molecule magnets and molecular qubits,” *Dalton Trans.* **49**(29), 9916–9928 (2020).
- <sup>66</sup>J. Bezanson, A. Edelman, S. Karpinski, and V. B. Shah, “Julia: A fresh approach to numerical computing,” *SIAM Rev.* **59**(1), 65–98 (2017).
- <sup>67</sup>J. H. Van Vleck, “Paramagnetic relaxation times for titanium and chrome alum,” *Phys. Rev.* **57**(5), 426–447 (1940).
- <sup>68</sup>S. Gómez-Coca, A. Urtizberea, E. Cremades, P. J. Alonso, A. Camón, E. Ruiz, and F. Luis, “Origin of slow magnetic relaxation in Kramers ions with non-uniaxial anisotropy,” *Nat. Commun.* **5**(1), 4300 (2014).
- <sup>69</sup>S. Demir, M. D. Boshart, J. F. Corbey, D. H. Woen, M. I. Gonzalez, J. W. Ziller, K. R. Meihaus, J. R. Long, and W. J. Evans, “Slow magnetic relaxation in a dysprosium ammonia metallocene complex,” *Inorg. Chem.* **56**(24), 15049–15056 (2017).
- <sup>70</sup>Y.-S. Ding, N. F. Chilton, R. E. P. Winpenny, and Y.-Z. Zheng, “On approaching the limit of molecular magnetic anisotropy: A near-perfect pentagonal bipyramidal dysprosium(III) single-molecule magnet,” *Angew. Chem., Int. Ed.* **55**(52), 16071–16074 (2016).
- <sup>71</sup>Y.-S. Ding, K.-X. Yu, D. Reta, F. Ortu, R. E. P. Winpenny, Y.-Z. Zheng, and N. F. Chilton, “Field- and temperature-dependent quantum tunnelling of the magnetisation in a large barrier single-molecule magnet,” *Nat. Commun.* **9**(1), 3134 (2018).
- <sup>72</sup>Y.-S. Ding, T. Han, Y.-Q. Zhai, D. Reta, N. F. Chilton, R. E. P. Winpenny, and Y.-Z. Zheng, “A study of magnetic relaxation in dysprosium(III) single-molecule magnets,” *Chem.-Eur. J.* **26**(26), 5893–5902 (2020).
- <sup>73</sup>C. P. Landee and E. F. Westrum, “Thermophysical measurements on transitionmetal tungstates II. Heat capacities of antiferromagnetic nickel and cobalt tungstates,” *J. Chem. Thermodyn.* **8**(5), 471–491 (1976).